FEASIBILITY AND EFFECTIVENESS OF A HIGHER HARMONIC CONTROL SYSTEM FOR A MEDIUM UTILITY HELICOPTER

Do-Hyung Kim, Korea Aerospace Research Institute, Daejeon, Korea
Jae-Sang Park, Chungnam National University, Daejeon, Korea
Shin-Won Bang, Chungnam National University, Daejeon, Korea

Abstract

The application of a Higher Harmonic Control (HHC) system for vibration reduction on a medium utility helicopter is under consideration. The HHC actuators are located between the main rotor actuator and the non-rotating swashplate. The higher harmonic variation of the blade pitch according to the N/rev higher harmonic motion of each HHC actuator is derived. The aeromechanical analysis model of the helicopter main rotor system is constructed using CAMRAD II, then the vibration responses with respect to the HHC actuator N/rev actuations are calculated to make a helicopter system model. Control authority of the HHC system to reduce vibratory hub loads is evaluated by closed-loop control simulations.

1. INTRODUCTION

Active rotor control has been studied since the 1950s [1]. A theoretical study of the Higher Harmonic Control (HHC) technique to mitigate the inherent problems of helicopters was first reported in 1952 [2]. It was suggested that the phenomenon of load redistribution on the rotor disk when a second harmonic control input is added to the primary control can be used to increase the forward flight speed limit caused by the stall of the retreating blade. The blade flapping and angle of attack changes due to the second harmonic control input were calculated theoretically, and the equation was verified by comparison with the test results. Starting with the Bell 212 flight using the HHC system in 1965, many studies were conducted in the 1970s and 1980s. In particular, vibration reduction studies using the HHC technique were actively conducted, but the HHC system was not yet applied to mass-produced helicopters. Since then, various studies have been conducted on vibration and noise reduction using the Individual Blade Control (IBC) technique, but this has not yet resulted in a system for production helicopters.

One of the reasons HHC technology has not been applied to production helicopters has been the lack of available low weight, high reliability actuators. With the recent development of electric motor and actuator technologies, an HHC system using small electro-mechanical actuators has become a challenging task. In order to develop an HHC system, it is necessary to study the applicability to the target aircraft, the effects of the system, and the required actuator control capability. In this paper, the feasibility and effectiveness of the HHC system for a medium helicopter are investigated by numerical simulation.

2. HELICOPTER MODEL

2.1. Baseline helicopter

The medium utility helicopter considered in this study is a four-bladed (7.9 m radius), twin-engine rotorcraft that carries up to nine armed troops along with a crew of four (two pilots and two gunners in the main cabin area) in a utility transport capacity. The maximum cruise speed is 150 knots and the service ceiling is 4,595 m. The maximum takeoff weight is 8,709 kg, but the operating weight is used as the nominal thrust condition in this study

2.2. CAMRAD II model

The comprehensive aeromechanics analysis code CAMRAD II is used to simulate the helicopter model. The blade structure is discretized into 8 nonlinear beam finite elements with 15 degrees of freedom each, including the contribution of rigid and elastic blade motions. The rotor control system including swashplates, pitch-links and pitch-horns is modeled in a sophisticated way. The rotor aerodynamic model used is based on the ONERA EDLIN unsteady theory with C81 airfoil table lookup. For the aerodynamic calculation, the blade is divided into 21 aerodynamic panels. A multiple-trailer wake model with consolidation is used to compute the non-uniform induced velocities around the rotor. The isolated rotor with HHC is trimmed to satisfy the given thrust, hub roll and pitch moments at the given flight speed and rotor shaft angle of attack. The geometry of the rotor system is shown in Figure 1.

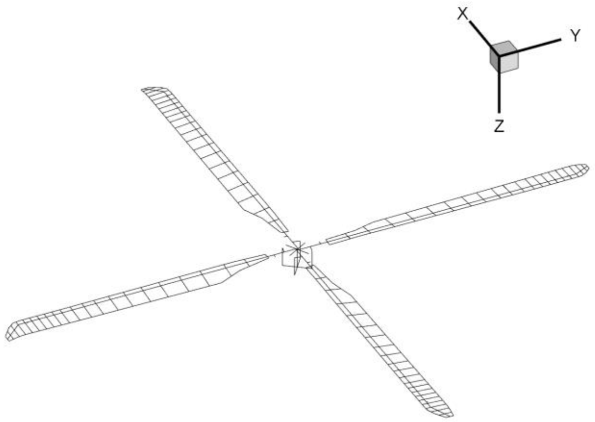

Figure 1: Geometry of CAMRAD II model.

2.3. Flight conditions

Level flight at 40, 60, and 80 knots at an altitude of 2,000 ft under international standard atmospheric conditions are used as baseline flight conditions. For simplicity, the isolated rotor system model in wind tunnel conditions was used. First, the rotor shaft tilt angles were obtained from the free flight trim conditions at each flight speed. Then, the analysis was performed under wind tunnel conditions for the isolated rotor model with the rotor shaft tilt angle was applied, and the vibratory hub loads were extracted.

3. HIGHER HARMONIC CONTROL SYSTEM

3.1. System architecture

The architecture of the HHC system is shown schematically in Figure 2. In steady state flight, the vibratory loads on the helicopter are periodic, with a fundamental frequency of N/rev in the nonrotating frame, where N is the number of blades. Harmonic analysis of the helicopter response is required to provide the vibration harmonics to the controller, and the m/rev (m = N, 2N, …) harmonic control command is calculated by the control algorithm and provided to the actuator controller. The HHC actuators then produce a nonrotating swashplate m/rev motion that causes m-1, m, m+1/rev blade pitch angle changes through the rotating swashplate and pitch-links.

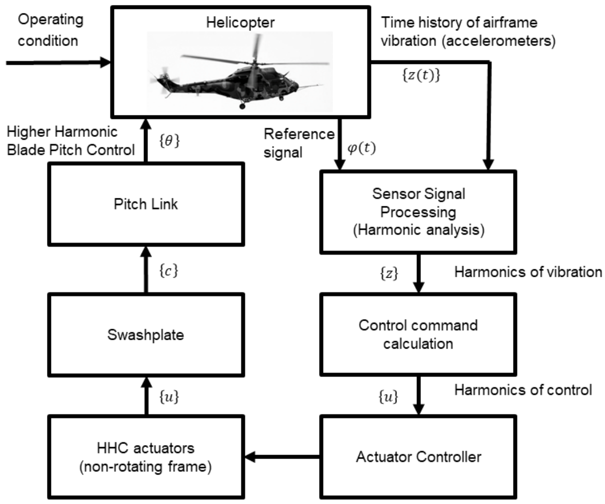

Figure 2: Architecture of an HHC system.

3.2. Relationship between actuator motion and blade pitch angle

The blade pitch angle changes according to the m/rev swashplate motion is derived in Ref. 3.

$$(1)\quad \begin{Bmatrix} \theta_{(m-1)c} \\ \theta_{(m-1)s} \\ \theta_{mc} \\ \theta_{ms} \\ \theta_{(m+1)c} \\ \theta_{(m+1)s} \end{Bmatrix} = \begin{bmatrix} 0 & 1/2 & 0 & 0 & 1/2 & 0 \\ -1/2 & 0 & 0 & 0 & 0 & 1/2 \\ 0 & 0 & 1 & 0 & 0 & 0 \\ 0 & 0 & 0 & 1 & 0 & 0 \\ 0 & -1/2 & 0 & 0 & 1/2 & 0 \\ 1/2 & 0 & 0 & 0 & 0 & 1/2 \end{bmatrix} \begin{Bmatrix} S_{LNG,c} \\ S_{LNG,s} \\ S_{COL,c} \\ S_{COL,s} \\ S_{LAT,c} \\ S_{LAT,s} \end{Bmatrix}_m$$

Equation (1) can be simply rewritten as:

$$(2)\qquad \{\theta\} = [H_1]\{S\}$$

The m/rev motion of the swashplate, $\{S\}$, generated by the m/rev motion of the actuator, can be described as:

$$(3)\qquad \{S\} = [H_2]\{u\}$$

where, $\{u\}$ is the HHC actuator control input vector representing the m/rev motion of the HHC actuators. Three HHC actuators are installed between the main rotor actuators and the nonrotating swashplate, and the actuators are excited by m/rev frequency. Thus, $\{u\}$ can be expressed as:

(4) $$\{u\} = [u_{1c} \quad u_{1s} \quad u_{2c} \quad u_{2s} \quad u_{3c} \quad u_{3s}]^T$$

The blade pitch angle changes with respect to the m/rev motion of the actuator can be obtained as:

(5) $$\{\theta\} = [H_1][H_2]\{u\} = [H]\{u\}$$

The relationship between the swashplate motion and the HHC actuator, $[H_2]$, can be found from the geometry of the rotor control system. The $[H_2]$ matrix was obtained by measuring the kinematic characteristics of the rotor system of the target helicopter, and the $[H]$ matrix was finally obtained by combining with the $[H_1]$ matrix.

3.3. Optimal control solution

The multicyclic vibration control algorithm [4, 5] is used in this study. The global model representation of the helicopter is as follows:

(6) $$z_n = z_0 + T u_n$$

where, z is the output vector of the sine and cosine components of the harmonics of the vibration, and u is the input vector of the harmonics of the actuator control. T is the transfer function representing the helicopter model, and the subscript n represents the n-th step. The control algorithm is based on the minimization of the performance function. The general form of the quadratic performance function is:

(7) $$J = z_n^T W_z z_n + u_n^T W_u u_n + \Delta u_n^T W_{\Delta u} \Delta u_n$$

where, $\Delta u_n = u_n - u_{n-1}$, W_z is the weighting matrix for the response, W_u is the weighting matrix for the multicyclic control input, and $W_{\Delta u}$ is the weighting matrix for the multicyclic control rate.

The optimal control input is found by substituting for z_n in the performance function and then solving for u_n that minimizes J. The general solution, which applies to both the local and global models, is as follows:

(8) $$u_n = C z_{n-1} + (C_{\Delta u} - CT) u_{n-1}$$

or $\Delta u_n = C z_{n-1} - C_u u_{n-1}$

where, $C = -DT^T W_z$, $C_{\Delta u} = D W_{\Delta u}$, $C_u = D W_u$, and $D = (T^T W_z T + W_u + W_{\Delta u})^{-1}$. For the global model, the optimal solution can be simplified as:

(9) $$u_n = C z_0 + C_{\Delta u} u_{n-1}$$

or $\Delta u_n = C z_0 - (C_u - CT) u_{n-1}$

3.4. Closed-loop control

Although, the equation (8) can be used in feedback control as it is, but the control command is suddenly changed to the optimal solution in one step for the global model with no estimation error, no measurement noise, and $W_{\Delta u} = 0$. Another method that minimizes the performance function by iteratively moving in the direction of the steepest descent can be used. The control command update equation of the gradient descent method is:

(10) $$u_{n+1} = u_n - \mu(T^T W_z z_n + W_u u_n + W_{\Delta u} \Delta u_n)$$

where, $\mu > 0$ is the step size or learning rate.

4. HIGHER HARMONIC CONTROL SIMULATION

4.1. Off-line system identification

For the simulation of the HHC system, the response output vector z and the control input vector u are defined. The 4/rev nonrotating hub forces, roll and pitch moments are used as the output vector because the baseline model is a 4-bladed isolated rotor system.

(11) $$z = [F_{x4c} \quad F_{x4s} \quad F_{y4c} \quad F_{y4s} \quad F_{z4c} \quad F_{z4s} \quad M_{x4c} \quad M_{x4s} \quad M_{y4c} \quad M_{y4s}]^T$$

The control input vector is equal to equation (4). The minimum number of the input-output data sets required for the system identification is equal to the number of control inputs, which is 6 for this study. However, 24 input-output cases are calculated for each flight condition in addition to the uncontrolled case. The data set consists of 50% and 100% amplitude and positive and negative direction excitation cases. Here, 100% amplitude is defined as the amplitude that produces a 2-degree change in blade pitch angle when the three actuators kinematically give a static collective motion. And negative direction excitation means the case where (-) Cosine or (-) Sine excitation is applied. The HHC actuator control input was converted to the higher harmonic blade pitch control input using equation (5), and then applied to the CAMRAD II calculation.

The analysis result for the baseline flight conditions in Figure 3 shows that the amplitude of the vibratory loads decreases with increasing flight speed, which is consistent with the characteristics of the aircraft.

The changes of the F_z component according to the excitation of actuator no. 1 is shown in Figure 4. It can be seen that the system response to the actuator input has good linearity.

The numerical system model $\hat{T}$ for the helicopter model T is calculated by the off-line system identification technique [4, 5]. A set of M (=24 in this study) test cases is used to obtain the transfer function model $\hat{T}$ using equation (12).

(12) $$\hat{T} = ZU^T(UU^T)^{-1}$$

where, Z is the response matrix containing M columns of the output z, and U is the input matrix containing M columns of control input u.

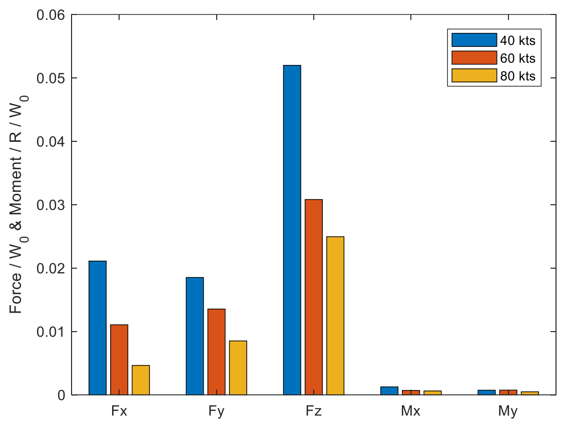

Figure 3: Vibratory loads of the baseline conditions.

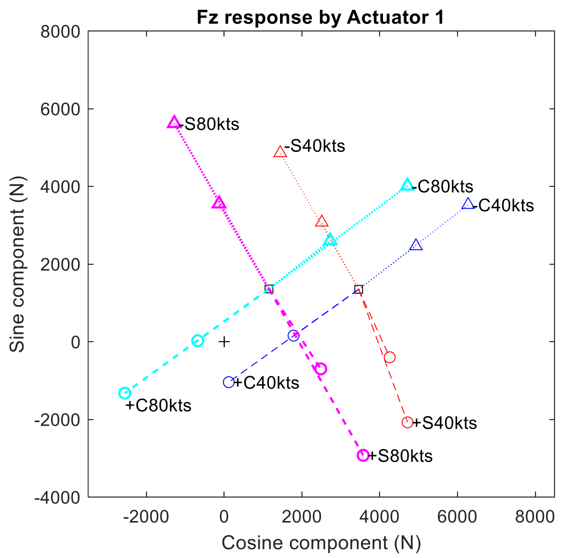

Figure 4: F_z response to actuator 1 excitation.

The system model for the 40-knot speed condition is shown as a bar graph in Figure 5. It appears that the F_z response appears relatively higher than other components.

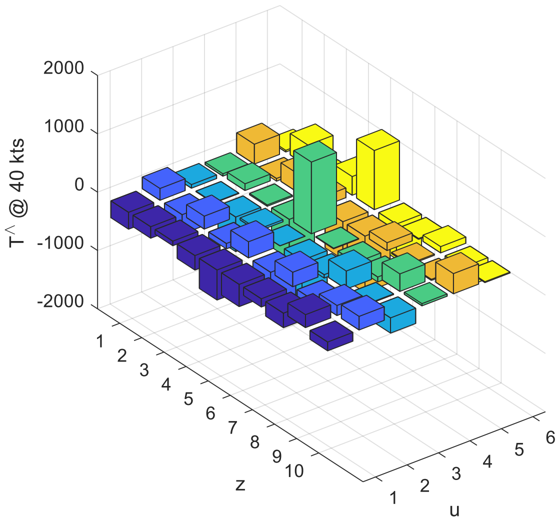

Figure 5: Identified system model at 40 knots.

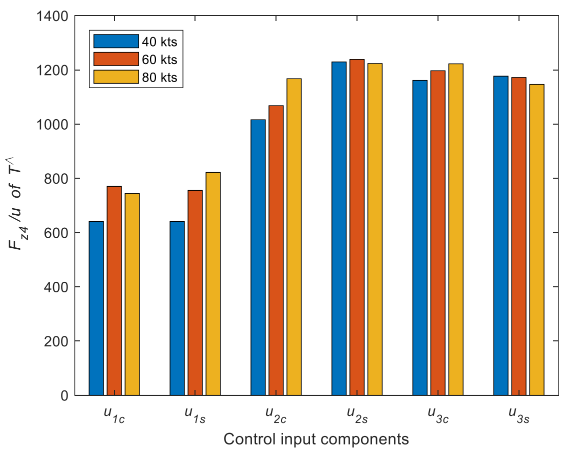

Figure 6: Magnitude of the F_{z4} responses to control input ($F_{z4} = \sqrt{F_{z4c}^2 + F_{z4s}^2}$).

Figure 6 shows the magnitude of the F_z response to the independent control input of the system model $\hat{T}$ at 40, 60, and 80 knots flight conditions. It can be seen that the F_z response by actuators 2 and 3 is larger than the response by actuator 1.

4.2. Fixed flight conditions

If there is no change in flight conditions, deterministic control can be applied. This means that the system model used in the control algorithm is fixed.

In order to obtain optimal solution, weight matrices must be defined. To simplify the objective function to the sum of squares of the vibratory loads, W_u and $W_{\Delta u}$ are set to zero. Then, the quadratic performance function is simplified as:

(13) $J = z_n^T W_z z_n$

The output response weight matrix W_z is defined so that the objective function has a form similar to the vibration index [6].

(14) $$VI = \frac{\sqrt{(0.5F_{x,4})^2 + (0.67F_{y,4})^2 + (F_{z,4})^2}}{W_0} + \frac{\sqrt{M_{x,4}{}^2 + M_{y,4}{}^2}}{RW_0}$$

The W_z is defined as:

(15) $$W_z = diag(\left(\tfrac{1}{2}\right)^2/W_0\,, \left(\tfrac{1}{2}\right)^2/W_0\,, \left(\tfrac{2}{3}\right)^2/W_0\,, \left(\tfrac{2}{3}\right)^2/W_0, \\ 1/W_0\,, 1/W_0\,, 1/RW_0\,, 1/RW_0\,, 1/RW_0\,, 1/RW_0)$$

Then the performance function becomes:

(16) $$J = \frac{(0.5F_{x,4})^2 + (0.67F_{y,4})^2 + (F_{z,4})^2}{W_0} + \frac{M_{x,4}{}^2 + M_{y,4}{}^2}{RW_0}$$

where, $(F_{x,4})^2 = (F_{x4C})^2 + (F_{x4S})^2$, R is the rotor radius, and W_0 is the operating weight of the target helicopter.

Since it is assumed that the flight condition does not change, a global model can be used. And, since $W_{\Delta u} = 0$ is applied, equation (9) is further simplified.

(17) $u_{opt} = Cz_0$

4.2.1. Open-loop control

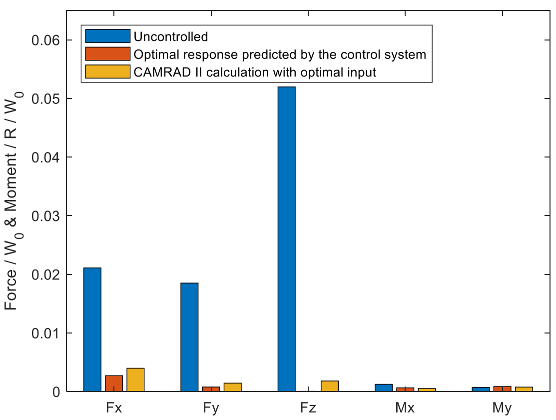

Figure 7: Linear system simulation and CAMRAD II calculation using the optimal control input at 40 knots.

The optimal solution for the 40 knots flight condition was calculated using equation (17), and the response to the optimal control input was calculated using equation (6). Then, CAMRAD II calculation using this optimal control input was also performed and compared with the result of the linear system control simulation in Figure 7. The most dominant component of the hub vibratory load, F_z, is greatly reduced, and the CAMRAD II calculation result is similar to that of the linear system simulation. Therefore, it can be seen that the off-line identified linear system model is a good representation of the helicopter model expressed in CAMRAD II.

The actuator displacements corresponding to the optimal solutions for 40, 60, and 80-knot flight conditions are shown in Figure 8. The largest actuator displacement is required for the 40-knot flight condition because the vibration is greatest at the low speed condition, as seen in Figure 3. Actuator 2 requires up to 50.6% of its operating range, while actuators 1 and 3 use less than 30% of their control authority. It can be seen that the HHC system has sufficient control authority within the flight condition considered in this study.

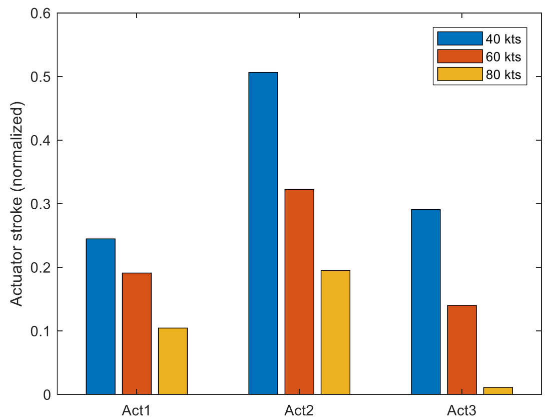

Figure 8: Actuator displacements required for optimal control.

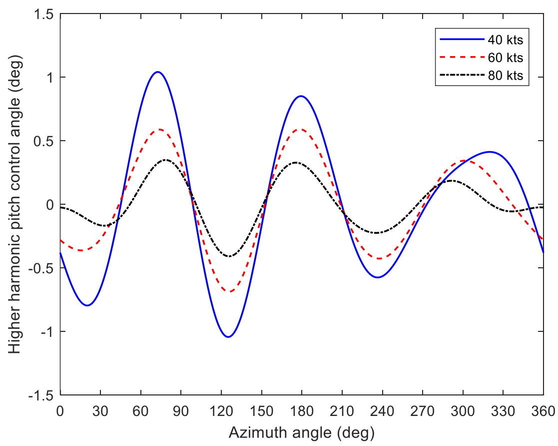

Figure 9: Higher harmonic blade pitch angle changes produced by optimal actuator control input.

The blade pitch angle changes corresponding to the optimal solutions can be calculated using equation (5). The higher harmonic blade pitch control input as a function of the azimuth angle is shown in Figure 9. At 40 knots, the magnitude of the higher harmonic blade pitch angle is ± 1.04 degrees, and as the flight speed increases, the higher harmonic blade pitch angle required for vibration reduction decreases. However, the overall waveform is similar. It should also be noted that the control amplitude is larger on the advancing side than on the retreating side.

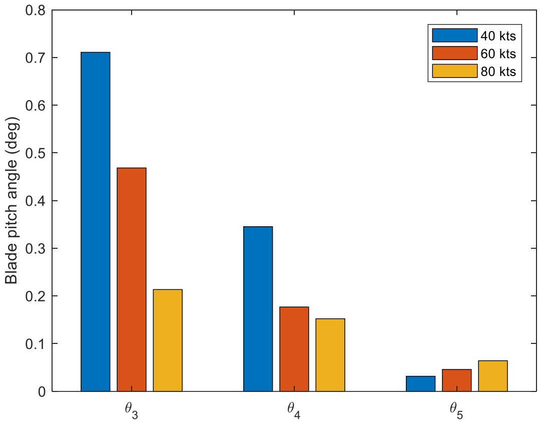

Figure 10: Harmonic components of the optimal blade pitch angles.

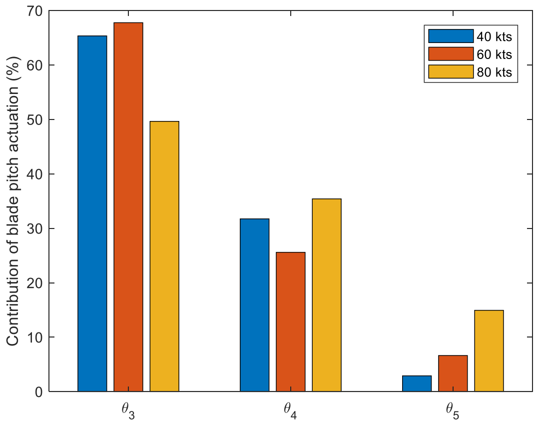

Figure 11: Percentage contribution of the blade pitch harmonic components in optimal solutions.

Figure 10 shows the optimal control inputs by harmonic components. It can be seen that the 3/rev component contributes the most to the optimal solution for vibration reduction, and the 5/rev component contributes the least. As the flight speed increases from 40 knots to 80 knots, the contribution of the 3/rev component decreases and the contribution of the 5/rev component increases slightly as shown in Figure 11, which represents the percentage contribution of the blade pitch control harmonic components in the optimal solution.

4.2.2. Closed-loop control

Closed-loop control simulation was performed using the gradient descent method expressed in equation (10). The system responses with respect to different step sizes at 40 knots flight condition are shown in Figure 12. As μ increases from 0.001 to 0.03, the convergence speed of the system increases. However, when μ is increased to 0.0425, the system diverges. Therefore, in the following simulations, $\mu = 0.01$ was used to consider the convergence speed and stability. When the system converges, the value of the cost function converges to the optimal solution as the time step increases.

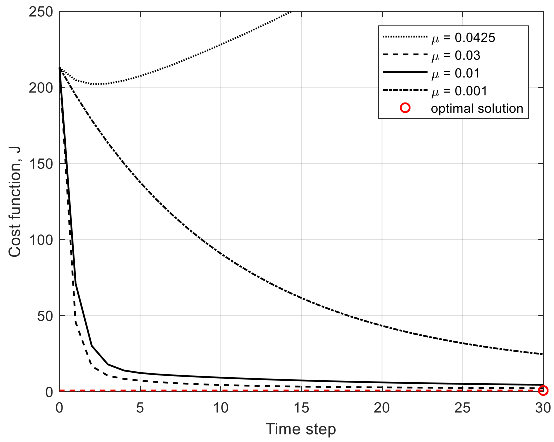

Figure 12: Performance of the HHC system at 40 knots as a function of step-size variations.

4.3. Flight conditions change

4.3.1. Speed change scenario

In order to simulate the situation where the flight conditions change, the case where the flight speed increases according to the time step is set as shown in Figure 13. It is assumed that the dynamics of the helicopter model changes linearly with the flight speed.

4.3.2. Open-loop control

When the open-loop control is applied using the optimal solution obtained at the 40-knot condition, the vibration reduction performance degrades as the system characteristics change with time, as shown in Figure 14. In this case, the system does not become unstable, but it can be clearly seen that it is not appropriate to use the optimal control input calculated at a different flight condition as the open-loop control input. It can be assumed that the reason why the system did not become unstable in this simulation is that the difference between the system model in the 40-knot condition and the 80-knot condition is not large. As shown in Figure 4, the system response characteristics to the actuator control input are very similar at both speeds.

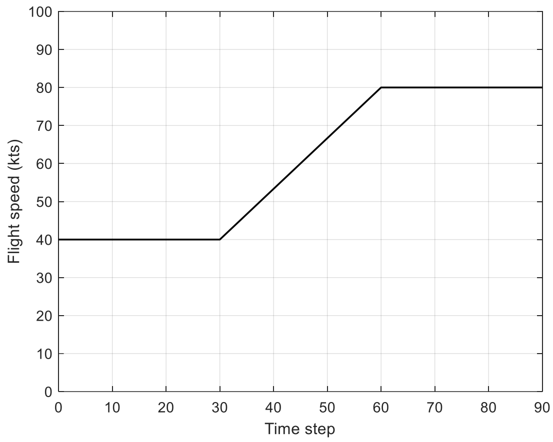

Figure 13: Flight speed change scenario.

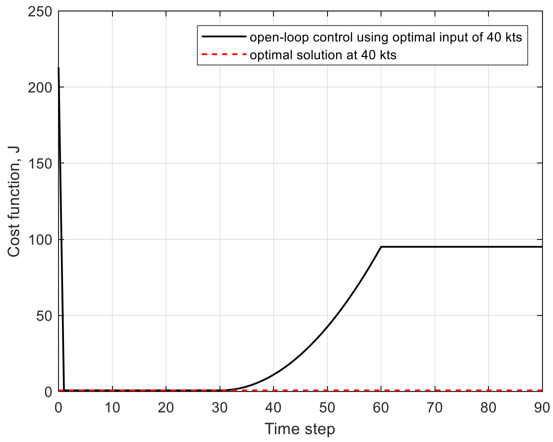

Figure 14: Open-loop control using the optimal solution at 40 knots under the flight speed change condition.

4.3.3. Closed-loop control by table lookup

One way to account for changes in flight conditions is to configure multiple system models in a lookup table. Then, the best system model suitable for the current flight condition can be selected and used.

A closed-loop control simulation was performed with the following lookup table criteria.

1) Speed = 0 ~ 60 knots : $\hat{T} = \hat{T}$ @ $40\ knots$

2) Speed = 60 knots ~ : $\hat{T} = \hat{T}$ @ $80\ knots$

The system model in the equation (10) changes when the flight speed increases above 60 knots. In this case, as shown in Figure 15, the vibration reduction performance is maintained without degradation. A lookup table can be used to consider not only the flight speed, but also various changes in flight conditions.

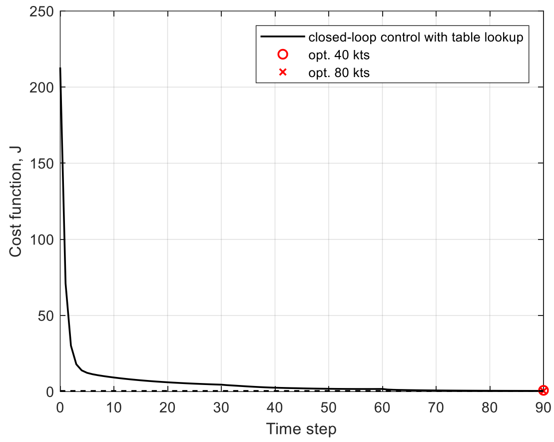

Figure 15: Closed-loop control simulation using table lookup technique.

4.3.4. Adaptive control

Among the methods for controlling time-varying systems, one of the most widely used is the adaptive control technique. Vibration control using the system model identified on-line at each time step based on the Kalman filter has been used [4,7].

The model characteristics are continuously updated with time, and a local model is used for on-line system identification. The helicopter model T is assumed to be linear about the current control inputs. The control inputs are based on the measured response. The general solution for the control inputs is equation (8) as described earlier. Assuming $W_u = W_{\Delta u} = 0$, the control input can be written as:

(18) $$\Delta u_n = C z_{n-1}$$

$$u_n = u_{n-1} + C z_{n-1}$$

Applying the step size used in gradient descent method, the control input becomes

(19) $$u_n = u_{n-1} + \mu C z_{n-1}$$

The feedback gain C gets updated with time via T. The Kalman estimation of T is given by

(20) $$\hat{T}_n = \hat{T}_{n-1} + \left(\Delta z_n - \hat{T}_{n-1} \Delta u_n\right) K_n^T$$

where,

$$\Delta z_n = z_n - z_{n-1}$$

$$K_n = \frac{P_n^- \Delta u_n}{\Delta u_n^T P_n^- \Delta u_n + R}$$

$$P_n^- = P_{n-1} + Q$$

$$P_n = P_n^- - K_n \Delta u_n^T P_n^-$$

and Q is the covariance of process noise, R is the covariance of measurement noise, P_n^- is the covariance of error in the estimate of T_n before measurement, and P_n is the covariance of error in the estimate of T_n after measurement. The superscript '-' indicates predicted value and the superscript '^' indicates the estimated value.

When applying the Kalman filter to the same flight speed change scenario described in Section 4.3.1, excellent performance can be achieved as shown in Figure 16 if the covariance of process noise, the covariance of measurement noise, and initial conditions are well chosen.

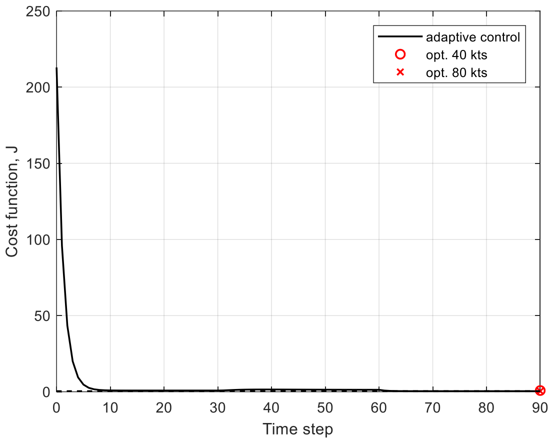

Figure 16: Closed-loop on-line control simulation using Kalman filter.

4.3.5. Deterministic control

When the system characteristics change over time, it is shown that excellent control performance can be maintained by using a table lookup or an adaptive control method. However, the use of lookup tables requires dealing with large system model data, and it is difficult to set the appropriate parameters needed to reliably use adaptive control. Therefore, it is worth investigating whether sufficient performance can be achieved by using a deterministic controller with a fixed system model.

As seen in Section 4.3.2, the system does not become unstable even when the optimal control input for the 40-knot condition is applied to the system at the 80-knot flight condition. From this, it can be expected that the closed-loop control using a fixed system model identified off-line at the specific flight condition will work well. The simulation result of the closed-loop control using the gradient descent method is shown in Figure 17. In this case, the fixed system model identified at 40-knot condition is used to calculate the control command by equation (10). It can be seen that the vibration control performance is excellently maintained even when the system characteristics change with the flight speed as shown in Figure 13. This simulation result confirms the validity of the assumption that the system characteristics at 40 knots and 80 knots are very close.

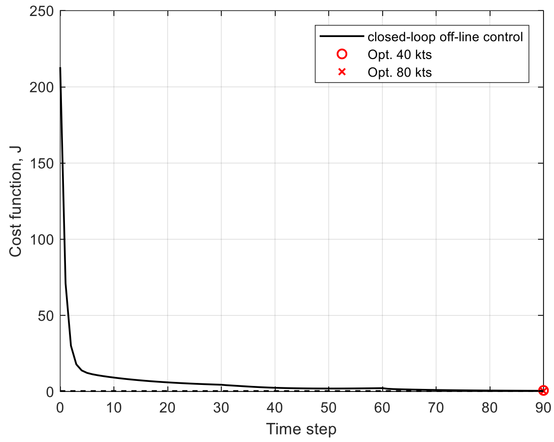

Figure 17: Deterministic control simulation using a fixed system model identified at 40 knots.

The control algorithm used in this study can be considered as a frequency domain FxLMS algorithm [8, 9]. The transfer function T corresponds to the forward path or cancellation path model. With regard to the cancellation path transfer function error and system stability, the contents of ref. 8 are as follows.

"If the phase error in the transfer function estimate exceeds 90 degrees (for a single channel system), the adaptive algorithm will become unstable. In practice, it is better to limit the error to less than 45 degrees. For multi-channel systems, the phase requirement surprisingly becomes less restrictive as the number of channels increases."

It can be seen that the deterministic controller can be used stably even if the identified system model is somewhat different from the actual system.

5. CONCLUSIONS

The feasibility and effectiveness of the HHC system for a medium helicopter are investigated by numerical simulation.

1. The HHC system shows effectiveness and the actuators have sufficient control authority for vibration reduction.
2. In the simulation conditions of this study, the largest vibration occurs at 40 knots, and the actuator displacement for vibration reduction is also the largest at this condition. As the flight speed increases, the magnitude of the HHC input required for vibration reduction decreases.
3. At 40 knots, actuator 2 requires up to 50.6% of its operating range, while actuators 1 and 3 use less than 30% of their control authority.
4. The control amplitude is larger on the advancing side than on the retreating side.
5. When system characteristics change over time, table lookup and adaptive control methods show excellent vibration reduction performance.
6. When the identified model does not differ significantly from the actual system, using a deterministic controller is the simplest and easiest method.

Author contact:

Do-Hyung Kim, dhkim@kari.re.kr

Jae-Sang Park, aerotor@cnu.ac.kr

Shin-Won Bang, tlsdnjs1009@gmail.com

6. ACKNOWLEDGMENTS

This work was supported by Korea Research Institute for defense Technology Planning and advancement (KRIT) grant funded by the Korea government (DAPA (Defense Acquisition Program Administration)) (No. KRIT-CT-21-020, Development of Higher Harmonic Control (HHC) SW for Helicopter Vibration Reduction, 2023).

7. REFERENCES

1. Kessler, C., “Active Rotor Control for Helicopters: Motivation and Survey on Higher Harmonic Control,” *CEAS Aeronautical Journal*, Vol. 1, (1–4), 2011, pp. 23–54.
2. Stewart, W., “Second Harmonic Control on the Helicopter Rotor,” R. & M. No. 2997, Aeronautical Research Council, 1952.
3. Biggers, J. C., and McCloud, J. L., III, “A Note on Multicyclic Control By Swashplate Oscillation,” NASA TM 78475, 1978.
4. Johnson, W., “Self-Tuning Regulators for Multicyclic Control of Helicopter Vibration,” NASA TP 1996, 1982.
5. Kim, D.-H., Hong, S., and Jung, S. N., “Multicyclic Vibration Control of a Helicopter Rotor with Active Twist Actuation,” 47th European Rotorcraft Forum, United Kingdom, 7-9th September, 2021.
6. van der Wall, B. G., Lim, J. W., Riemenschneider, J., Kallow, S., Wilke, G. A., Boyd, D. D. Jr., Bailly, J., Delrieux, Y., Cafarelli, I., Tanabe, Y., Sugawara, H., Jung, S. N., Hong, S. H., Kim, D.-H., Kang, H. J., Barakos, G., and Steininger, R., “Smart Twisting Active Rotor (STAR) – Pretest Predictions,” 48th European Rotorcraft Forum, Winterthur, Switzerland, 6-8 September 2022.
7. Chopra, I., and McCloud, J. L., III, “A numerical Simulation Study of Open-Loop, Closed-Loop, and Adaptive Multicyclic Control Systems,” *Journal of the American Helicopter Society*, Vol. 28, (1), Jan. 1983, pp. 63-77.
8. Hansen, Colin H., *Understanding Active Noise Cancellation*, Spon Press, London, 2001, Chapter 3.
9. Kim, D.-H., Kwak, D.-I, and Song, Qi, “Demonstration of Active Vibration Control System on a Korean Utility Helicopter,” International Journal of Aeronautical and Space Sciences, Vol. 20, (1), 2019, pp. 249–259. DOI: 10.1007/s42405-018-0106-3